Seasonal characterization of CDOM for lakes in semi-arid regions of Northeast China using excitation-emission matrices fluorescence and parallel factor analysis (EEM-PARAFAC)

Ying Zhao[1], Kaishan Song[1*], Zhidan Wen[1], Lin Li[2], Shuying Zang[3], Tiantian Shao[1], Sijia Li[1], Jia Du[1]

[1]Northeast Institute of Geography and Agroecology, Chinese Academy of Sciences, Changchun, Jilin, 130102, China

[2]Department of Earth Sciences, Indiana University-Purdue University, Indianapolis, IN, USA

[3]College of Geographical Science, Harbin Normal University, Harbin, China

*corresponding author E-mail: songks@iga.ac.cn; Tel: 86-0431-85542364

Abstract. The seasonal characteristics of fluorescent components in CDOM for lakes in the semi-arid region of Northeast China were examined by excitation-emission matrix (EEM) spectra and parallel factor analysis (PARAFAC). Two humic-like (C1 and C2) and the protein-like (C3 and C4) components were identified using PARAFAC. The average fluorescence intensity of the four components differed under seasonal variation from June and August 2013 to February and April 2014. Components 1 and 2 exhibited strong linear correlation (R^2 = 0.633). Significantly positive linear relationships between CDOM absorption coefficients a(254) (R^2 = 0.72, 0.46, $p < 0.01$), a(280) (R^2 = 0.77, 0.47, $p < 0.01$), a(350) (R^2 = 0.76, 0.78, $p < 0.01$) and F_{max} for two humic-like components (C1 and C2) were exhibited, respectively. A

significant relationship ($R^2 = 0.931$) was found between salinity and DOC. However, almost no obvious correlation was found between salinity and EEM-PARAFAC extracted components except for C3 ($R^2 = 0.469$). Results from this investigation demonstrate that the EEM-PARAFAC technique can be used to evaluate the seasonal dynamics of CDOM fluorescent components for inland waters in the semi-arid regions of Northeast China, and to quantify CDOM components for other waters with similar environmental conditions.

Keywords: CDOM, fluorescent components, EEMs, PARAFAC, DOC, Salinity

1 Introduction

Dissolved organic matter (DOM), a heterogeneous mixture of humic acids, proteins and carbohydrates, plays important roles in aquatic ecosystems (Zhang et al., 2010). Chromophoric dissolved organic matter (CDOM), the colored fraction of DOM, absorbs light energy in the ultraviolet (UV) and visible region of the spectrum and inhibits the propagation of UV radiation. CDOM in waters also affects the transport and bio-availability of materials such as trace metals and other pollutants (Song et al., 2013), so it can be used as a proxy of water quality. In natural water bodies, CDOM originates from the degradation of plant materials and other organisms and terrestrially imported substances, which varies in time and space and is controlled by its structure and composition (Stedmon et al., 2003). CDOM is compositionally complex, making it difficult to isolate hydrophobic from hydrophilic acids using XAD ion-exchange resins (Aiken et al., 1992; Spencer et al., 2010). Nonetheless, some

46 optically active components of CDOM can emit fluorescence after absorbing light at
47 certain wavelengths (Zhang et al., 2010) so that the fluorescence spectroscopic
48 techniques can be used to provide detailed information about the source and
49 concentration of CDOM. The traditional fluorescence techniques including
50 fluorescence emission spectrometry and synchronous fluorescence scanning applied
51 to examine CDOM components have the drawback that the output was restricted to a
52 linear scan (Hudson et al., 2007).

53 Recently, excitation-emission matrix fluorescence spectroscopy (EEM) has been
54 applied to identify CDOM components because of its ability of producing
55 synchronous scan spectra in the form of contours (Stedmon et al., 2003; Zhang et al.,
56 2010). The EEM spectroscopy is considered the most effective technique for studying
57 the composition of fluorophores given its high selectivity and sensitivity to CDOM in
58 water columns (Zhang et al., 2010). In recent years, EEM spectroscopy has been
59 widely used to investigate the dynamics of marine, freshwaters and ice-water
60 ecosystems as well as snow melting water (Barker et al., 2006, 2009, 2010, 2013;
61 Coble, 2007; Fellmanet al., 2010; Guo et al., 2010; Hudson et al., 2007; Stedmon et
62 al., 2007). Moreover, the EEM spectroscopy can also be used to distinguish
63 allochthonous and autochthonous CDOM source in aquatic environment (Coble et al.,
64 1998; Mayer et al., 1999; Yamashita et al., 2008, 2010; Zhang et al., 2013). Based on
65 the peak positions in EEMs, two main fluorescent components, i.e., humic-like and
66 protein-like substances, have been identified and investigated (DelCastillo et al., 1999;
67 Jaffe´ et al., 2004). However, overlapped fluorophores of CDOM EEMs could make

68 this traditional ‘peak-picking’ method unreliable to evaluate CDOM dynamics in
69 aquatic ecosystems (Coble, 1996; Stedmon et al., 2003). Recently, the combined
70 EEMs-PARAFAC (parallel factor analysis) technique has been shown to effectively
71 decompose EEM of CDOM into independent fluorescent components and assess the
72 source of CDOM and relationships with other water quality parameters. A number of
73 investigators have used EEMs-PARAFAC to characterize DOM in freshwater and
74 marine aquatic environments (Broisover et al., 2009; Cory et al., 2005; Guo et al.,
75 2010; Stedmon et al., 2003; Stedmon and Markager, 2005; Yamashita, 2008; Zhang et
76 al., 2010, 2011, 2013). Stedmon et al. (2003) introduced PARAFAC and identified
77 five distinct DOM components for a Danish estuary and its catchment. In coastal
78 environments, Yamashita et al. (2008) reported on seven components using the
79 combined EEMs-PARAFAC technique and assess the dynamic of individual
80 fluorophores and relationship with salinity in Ise Bay. Zhang et al. (2011) also found
81 three different components by PARAFAC modeling and analyzed the correlations
82 between the fluorescent components and absorption coefficients of CDOM for Lake
83 Tianmu and its catchment.

84 The Songnen Plain is a fluvial plain with semi-arid climate, in which many fresh
85 and brackish waters are distributed according to its geomorphological characteristics
86 (Song et al., 2013). Dissolved organic carbon (DOC) characterisitics of these fresh
87 and brackish waters across the Songnen Plain have been studied by Song et al. (2013);
88 the results indicated that a huge amout of DOC were stored in these waters. In
89 particular, brackish waters would exhibit high average DOC concentration and

90 significantly contributed the carbon budget to inland waters (Duarte et al., 2008; Song
91 et al., 2013; Tranvik et al., 2009). However, little study has been made on the detailed
92 information of DOC sources for these waters in the Songnen Plain. Therefore, it
93 motivated us to investigate the components in CDOM for both fresh and brackish
94 waters in the semi-arid region. In the present study, the absorption and fluorescence of
95 CDOM were determined for the water samples collected from seven lakes in the
96 western part of Jilin province, which varied at different season. The specific
97 objectives of this study are to: 1) characterize CDOM components contained in these
98 lakes using EEMs and their origins through the EEM-PARAFAC method; 2) assess
99 the dynamic of individual fluorescent component of CDOM under seasonal variation;
100 and most importantly 3) link CDOM fluorescence intensities, absorption coefficients,
101 DOC concentrations and salinity to each other, in order to establish proxies for
102 CDOM bioavailability and photoreactivity in waters.
103

104 # 2 Materials and Methods

105 ## 2.1 Lakes and water sampling

106 The water bodies investigated in this study were located in the western part of Jilin
107 Province, which belongs to the semi-arid part of the Songnen Plain (Song et al., 2013).
108 Two groups of lakes were investigated, i.e., the Chagan lake group and the Yuelianghu
109 lake group. The Chagan lake group is made up of Lake Chagan (CGL), Xinmiaopao
110 (XMP), Xindianpao (XDP) and Kulipao (KLP). The Yuelianghu lake group mainly
111 includes Lake Yueliang (YLL), Talahong (TLH) and Xinhuangpao (XHP) (Fig. 1).

The two groups are about 60 km away from each other, of which each includes both fresh and brackish waters. The primary economic value for these lakes is fishery, agricultural irrigation and recreation. The average annual precipitation is about 391 mm, but the average evaporation is up to 1790 mm, resulting in water scarcity. Due to the area dominated by saline-alkali soil, the rainfall flush and agricultural catchment land use can result in an increase of lake salinities. These seven lakes are endowed with similar geological, hydrological and climatic settings, thus we presume that similar process may control the CDOM components. In order to characterize the CDOM fluorescent components under seasonal variation using EEMs-PARAFAC, 67 water samples were collected from the surface of the seven lakes in 1-liter acid-cleaned plastic bottles during four field campaigns in June and August 2013 as well as in February and April 2014, respectively. These samples were collected during the ice covering period using an ice drilling auger. The under-ice surface water was coming up when the ice layer was drilled a hole by the auger. The ice shavings were collected in plastic bags and the under-ice surface water was collected in plastic bottles. The collected samples were held on ice and immediately transported to the laboratory in the Changchun City of Jilin province within 3-5 hours. In the laboratory, these samples were filtered within 24h and then kept at 4 ℃ until analysis within two days. Latitude and longitude of each sample location were recorded *in situ* using a Trimble Global Positioning System (GPS).

Figure 1. Locations of the water sampling sites for 7 lakes in the western part of Jilin province, Northeast China.

2.2 Analytical procedures

To characterize the basic parameters of water quality, salinity was measured through a DDS-307 electrical conductivity (EC) meter in laboratory. Salinity was expressed in the basis of the UNESCO practical salinity unit (PSU 1978). The pH was measured using a PHS-3C pH meter at room temperature (20 ± 2 ℃) in laboratory. Water turbidity was determined using the Shimadzu UV-2600PC UV-Vis dual beam spectrophotometer with matching 3 cm quartz cells at room temperature (20 ± 2 ℃) with Milli-Q water as the reference (UV talk letter vol. 10, https://shimadzu.com.au/uv-talk-letter-volume-10). To determine DOC concentrations, water samples were filtered through 0.45 μm filters and then measured using a Shimadzu TOC-5000 Analyzer and a 1.2 % Pt on silica catalyst at 680 °C. Potassium hydrogen phthalate was used as standard. The reproducibility of the analytical procedure was within 2-3 % for the current study (APHA, 1998; Song et al., 2011).

2.3 Absorption measurement

In laboratory, all the samples were filtered at low pressure, first through a pre-combusted Whatman GF/F filter (0.7 μm), and then through a pre-rinsed 25 mm Millipore membrane cellulose filter (0.22 μm) into glass bottles. Absorption spectra of the samples were measured between 200 and 800 nm at 1 nm increments using the Shimadzu UV-2600PC UV-Vis dual beam spectrophotometer with a 1 cm quartz cuvette and Milli-Q water as reference. The absorption coefficient a_{CDOM} was

157 calculated from the measured optical density (OD) of the sample using Eq. (1):

158 $$a_{CDOM}(\lambda) = 2.303\left[OD_{(\lambda)} - OD_{(null)}\right]/\gamma \quad (1)$$

159 where γ is the cuvette path length (0.01 m) and the factor 2.303 converts from base 10
160 to base natural logarithm transformation. Some fine particles possibly remained in the
161 filtered solution (Babin et al., 2003; Bricaud et al., 1995), therefore it was necessary
162 to correct for scattering by fine particles and in this case, $OD_{(null)}$ is the average optical
163 density over 740-750 nm where the absorbance of CDOM can be assumed to be zero.

164 A CDOM absorption spectrum ($a_{CDOM}(\lambda)$) can be expressed as an exponential
165 function (Babin et al., 2003; Bricaud et al., 1995):

166 $$a_{CDOM}(\lambda_i) = a_{CDOM}(\lambda_r)\exp[-S(\lambda_i - \lambda_r)] \quad (2)$$

167 where $a_{CDOM}(\lambda_i)$ is the CDOM absorption at a given wavelength λ_i, $a_{CDOM}(\lambda_r)$ is the
168 absorption estimate at the reference wavelength λ_r(440 nm), and S is the spectral
169 slope of the CDOM absorption. According to Helms et al. (2008), S is calculated by
170 fitting a linear model to the date over a wavelength range of 275 to 295 nm (*S1*) or
171 350 to 400 nm (*S2*). To eliminate the inter-laboratory variability, the slope ratio S_R=
172 *S1*/*S2* is defined to indicate the molecular weight and photo-bleaching of CDOM
173 (Helms et al., 2008; Zhang et al., 2010).

174

175 **2.4 Three-dimensional fluorescence measurement**

176 The EEMs analysis of CDOM were conducted using a Hitachi F-7000 fluorescence
177 spectrometer (Hitachi High-Technologies, Tokyo, Japan) with a 700-voltage xenon
178 lamp. The scanning ranges were 200–450 nm for excitation, and 250–500 nm for

emission. Readings were collected in the ratio mode at 5 nm intervals for excitation, and at 1 nm intervals for emission, using a scanning speed of 2400 nm min^{-1}. The band-passes were 5 nm for both excitation and emission. A Milli-Q water blank of the EEMs was subtracted to eliminate the water Raman scatter peaks (McKnight et al., 2001; Stemdon et al., 2003; Zhang et al., 2010, 2011).

The inner-filter effect, which results from reabsorption and excitation of the fluorescence itself, can reduce the fluorescence intensity by 5% (Larsson et al., 2007; McKnight et al., 2001). In order to eliminate the inner-filter effect, the EEMs were corrected for absorbance by multiplying each value in the EEMs with a correction factor based on the assumption that the average path length of absorption of the excitation and emission light is one-half length of the cuvette (McKnight et al., 2001; Zhang et al., 2010). The correction function is expressed as follows:

$$F_{corr} = F_{obs} \times 10^{(A_{ex}+A_{em})/2} \quad (3)$$

where F_{Corr} and F_{obs} are the corrected and uncorrected fluorescence intensities and A_{ex} and A_{em} are the absorbance values at the respective excitation and emission wavelengths.

The measured fluorescence intensity is dependent on the concentration of the dissolved fluorophores in water bodies. Finally, the fluorescence intensities of all sample's EEMs were normalized to the area under the Milli-Q water Raman peak (λex=350 nm, λem=371-428 nm) measured daily (Lawaetz and Stedmon, 2009). The contour figures of the EEMs were plotted using the Matlab 10.0 software package

(Math Works, Natick Massachusetts, America).

2.5 The PARAFAC modeling

PARAFAC, a three-way method, is applied to decompose the CDOM fluorescence into separate fluorescent signals (Andersen and Bro, 2003; Stedmon and Bro, 2008). According to Stedmon and Bro (2008), a similar PARAFAC analysis is carried out in the present study using the DOMFluor toolbox in MATLAB with the "N-way toolbox for MATLAB" (Andersson et al., 2000). Before PARAFAC modeling, the excitation wavelengths from 200 to 220 nm and the emission wavelengths from 250 to 300 nm were deleted because of their poor quality. In order to remove the effect of Rayleigh scatter on PARAFAC modeling, the missing values (NaN-Not a number) were inserted in the regions (Ex-20 ≦ Em ≦ Ex+20 and 2Ex-20 ≦ Em ≦ 2Ex+20; unit: nm) which are significantly influenced by the first and second order scattering from the measured spectroscopic data (Hua et al., 2007; Stedmon and Bro, 2008).

To determine the appropriate number of PARAFAC components, the split-half validation procedure was executed to verify whether the model was valid by comparing the emission and excitation loadings from each half (Stedmon and Bro, 2008). Split-half analysis is the most effective method for implementing the PARAFAC models, in which the EEMs are randomly divided into four groups of equal size, and then analyzed for two half splits (1-2 and 3-4 half) respectively. If the correct number of components is chosen, the excitation and emission loadings from the two groups should show the same shape and size (Bro, 1997, 1999). The

fluorescence intensity of every component was represented by F_{max} (Raman unit: nm^{-1}) (Stedmon and Markager, 2005).

2.6 Statistical analysis

Statistical analysis was conducted using the SPSS 16.0 software package (Statistical Program for Social Sciences). Regression and correlation analysis was used to describe the relationship between CDOM absorption coefficient, DOC concentration, salinity and F_{max}. A model II-ANOVA was performed to determine seasonal variability is higher than between-lake variability. The difference is considered to be statistically significant when *p*-values are less or equal to 0.05.

3 Results and discussion

3.1 Water quality conditions

The water quality parameters, i.e., pH, salinity, turbidity for the 67 water samples collected from June 2013 to April 2014 in the western part of Jilin province are displayed in Table 1. When the set of samples from various field trips was pooled together, the waters had high pH values and high salt contents. The highest salinity was present when the lakes were frozen in February 2014, whereas relatively constant values (around 0.40 PSU) were exhibited in other three seasons. Also the water bodies were highly turbid. The highest turbidity was present in June 2013, and then reduced in August 2013, and the lowest value was recorded in February 2014. Compared with February 2014, the turbidity had almost no change in April 2014 (Table 1).

Table 1. Mean value of water quality parameters from June 2013 to April 2014.

3.2 EEMs characterization of CDOM

Based on the EEMs 'peak picking' technique, the key fluorescence peaks can be observed in 67 water samples: two humic-like and two protein-like substances (Coble, 1996; Stedmon et al., 2003). The humic-like components are the mixture of aromatic and aliphatic compounds-humic-like acids from terrestrial substances, and aquatic humic-like substances of phytoplankton origin. With respect to the protein-like components, they, i.e., tyrosine-like and tryptophan-like substance, mainly consist of dissolved amino acids. As an example, Fig. S1 displays the EEMs of samples from lake Xindianpao at different seasons. The peaks comprise two humic-like fluorescence peaks: one in the ultraviolet range (Ex/Em = 220-240/410-430 nm) and the other in the visible range (Ex/Em = 300-340/410-450 nm) and the protein-like fluorescence peaks: tyrosine-like (Ex/Em = 210-230, 270-280/310-330 nm) and tryptophan-like (Ex/Em = 220-230, 280-300/350-370 nm).

In our study, four separate fluorescent components (Fig. 2a-d) and the excitation and emission loadings (e-h) of the four components identified by EEM-PARAFAC are summarized in Fig. 2 and Table 2. The first fluorescent component (C1) was a biological degradation humic-like component comparable to humic-like peaks (M and N) in marine and in phytoplankton degradation experiments

for inland waters (Coble, 1996; Zhang et al., 2009). Component 2 was consistent with the humic-like peaks (A and C) defined by Coble (1996). Component 3 resembles the tryptophan-like (T) component as found by Baker et al. (2004) and Hudson et al. (2007). For component 4, it is likely related to tyrosine-like component (B) (Hudson et al., 2007). Components 3 and 4 represent autochthonous semi-labile CDOM associated with bacteria activity and phytoplankton degradation (Borisover et al., 2009; Stedmon et al., 2003). Particularly, there was a shoulder at the excitation wavelength 310-330 nm in component 3 and 330-340 nm in component 4, which may be due to the residual Raman peaks in some water samples (Fig. 2c-d). In this study, not all of the four components were present in all of the samples.

Figure 2. The PARAFAC modeling output shows the contour plots of the four PARAFAC fluorescent components (a-d) and excitation (black) and emission (red) loadings (e-h) of each component. Fluorescence is in Raman units: nm^{-1}.

Table 2. Positions of the fluorescence maximum peaks of the four components identified by PARAFAC modeling in the present study compared with those previously identified. Secondary excitation maxim is given in brackets.

3.3 Temporal distribution of PARAFAC components

These fresh and brackish water in Jilin province in northeast China are endowed with similar geological, hydrological and climatic settings, thus it is presumed that similar process may control the CDOM components. When a model II-ANOVA using season and lake as random effect factors was performed, it shows that the seasonal variability

($F > F_{crit}$, $p < 0.05$) is higher than between-lake variability. Therefore, the water samples from different lakes for every season were pooled together in order to study the seasonal variation of the fluorescent components. As shown in Fig. 3a, the average fluorescence intensity of the four components had seasonal variation. When all the water samples at different seasons were pooled together, the average value of total fluorescence intensity was 2.05 ± 0.93 nm^{-1}, corresponding to the intensities of 0.71 ± 0.32 (C1), 0.33 ± 0.11 (C2), 0.50 ± 0.24 (C3), and 0.51 ± 0.26 (C4) nm^{-1} for different components. These results can demonstrate that the fluorescence intensity was dominated by C1, implying most part of the CDOM for the seven inland lakes was originated from the degradation of phytoplankton and microorganisms. The protein-like components (C3 and C4), related to bioavailability and microbial activity of CDOM, had almost the same magnitude. At all four seasons, the fluorescent component C2, which was terrestrially imported to water bodies, contributed less to total fluorescence than the other three. The total fluorescence intensity differed under seasonal variation, varying from 2.54 ± 0.68 nm^{-1} in June to 1.93 ± 0.70 nm^{-1} in August 2013, and then increased to 2.34 ± 0.92 nm^{-1} in February and reduced to the lowest 1.57 ± 0.55 nm^{-1} in April 2014 (Fig. 3c). The intensities of four fluorescent components (i.e., 0.75 ± 0.17 (C1), 0.32 ± 0.06 (C2), 0.69 ± 0.24 (C3), and 0.77 ± 0.20 (C4) nm^{-1}) (Fig. 3d) from the samples collected in June 2013 exhibited similar trends to that for the pooled data set. These values were higher than the seasonal average except C2 (0.32 ± 0.06 nm^{-1}). This can be explained by enhanced activities from plant degradation and microbial activities, but less terrestrial substances were

313 imported to the water bodies in June and therefore the fluorescence intensity of C2
314 was lower than the seasonal average. Compared to the fluorescence intensity in June,
315 the three fluorescence intensities (0.65 ± 0.14 (C1), 0.33 ± 0.16 (C3), 0.52 ± 0.36 (C4)
316 nm^{-1}) from the samples collected in August 2013 reduced, but an increased value was
317 recorded for C2 (0.42 ± 0.05 nm^{-1}) (Fig. 3d). Especially, the fluorescence intensities
318 of two protein-like components showed an obvious difference. This can be attributed
319 to substantially increased precipitation up to 180 mm in July from June to August
320 2013 (Fig. 3b) so that flood occurred when rainfall continued to increase in August.
321 Gradually, DOM contained in terrestrial CDOM was flushed by rainfall to the lakes so
322 that the C2 (0.42 ± 0.05 nm^{-1}) fluorescence intensity became higher. In accordance
323 with Cheng et al. 2010, the rainwater CDOM for this study was largely characterized
324 by protein-like components (Cheng et al., 2010). The fluorescence intensity of the
325 rainwater CDOM was very weak, and also the rainwater CDOM contained much
326 lower humic-like concentration (Fig. S2b). The intensities of the other three
327 components decreased because of dilution resulting from heavy rain and relatively
328 weak microbial decomposition of plants.

329 The highest C1 (1.02 ± 0.38 nm^{-1}) presented in February 2014 and the C2 (0.39
330 ± 0.12 nm^{-1}) intensity remained almost the same as that in August 2013. However, the
331 protein-like components indicated that the C3 (0.57 ± 0.25 nm^{-1}) intensity was higher
332 than the C4 (0.35 ± 0.17 nm^{-1}) intensity, which was opposite to the results from other
333 months (Fig. 3d). In cold winter, the surface waters formed a thick layer of ice
334 covering the lake waters. Because the ice cover reduced light penetration and

restricted gas exchange between the underlying water and atmosphere, vigorous biological activities in the lakes would be reduced at low temperature and low light level (Thomas K., 1983; Uusikiv et al., 2010; Wharton, et al., 1993). Although the biological activities was very weak, there still be a bit of production of C1 and C3 in lake water. Also, dissolved materials were left in the underlying surface waters and little terrestrial matters were imported to the lakes once covered by ice (Stedmon et al., 2007). Therefore, the C1 and C3 in the water of the lakes beneath the ice layers would be produced and cumulated simultaneously, whereas, the C2 remained the same. Obviously, the fluorescence intensity of component 1 reached the highest value for the winter samples. As shown in Fig. S2a, another striking feature for the winter samples was that the fluorescence of CDOM in the ice was dominated by the tyrosine-like C4 component, which is consistent with the findings of Barker et al. (2009, 2013) and Stedmon et al. (2007). It showed that the C4 component was left in the ice-cover when the lakes were frozen. Therefore, it is not surprising that the intensity of component C4 for water beneath ice layers was reduced and the concentrated C3 showed a much higher fluorescence intensity. In April 2014, the intensities of four fluorescent components (0.47 ± 0.17 (C1), 0.25 ± 0.08 (C2), 0.40 ± 0.16 (C3), and 0.45 ± 0.13 (C4) nm^{-1}) (Fig. 3d) exhibited similar seasonal trends though these values were much lower than the average. Our interpretation is that the ice CDOM was characterized by tyrosine-like component (C4) (Fig. S2a), and the fluorescence intensity of C4 contributed by the ice-melt water was very weak. However, the underlying lake CDOM included both humic-like (C1 and C2) and

protein-like (C3 or C4) components. When the ice in the lakes melt into water with warming weather and biological degradation and human activity was weak, the lake CDOM was diluted by the ice-melted water and the fluorescence intensity would reach to the lowest value in early spring.

Figure 3. a) Seasonal average of F_{max} for EEM-PARAFAC components (C1, C2, C3 and C4) for lakes in the western part of Jilin province; b) Monthly variation of rainfall for the lakes in western part of Jilin province from April 2013 to February 2014; c) Seasonal variation of the total fluorescence intensity at different seasons; d) Seasonal variation of the four EEM-PARAFAC components at different seasons. The error bar represents standard deviations.

3.4 CDOM versus EEM-PARAFAC extracted components

The concentration of DOC, CDOM absorption coefficients and the slope ratio S_R are shown in Table 3. The DOC concentrations ranged from 10.03 to 56.60 mg L^{-1} with an average value of 31.66 mg L^{-1} during the study period from April to August 2013, demonstrating a seasonal dynamics that can be attributed to hydrological, climatic and landscape variations (Song et al., 2013). It is because the prolonged sunshine duration can result in an evapo-condensed DOC concentration in the Songnen Plain. The highest averaged DOC concentration (55.04 ± 20.00 mg L^{-1}) was present in February 2014; whereas, relatively constant values of approximate 30 mg L^{-1} were observed in the other three seasons. This can be attributed to the accumulated DOC when the lakes freeze in winter, which leaves DOC in the liquid phase, resulting in a higher DOC concentration in the underlying water (unpublished material). Generally, the

absorption coefficient a(350) is used as a proxy for characterizing CDOM concentration (Guo et al., 2010; Zhang et al., 2011). a(280) is related to DOC biodegradation (McDowell et al., 2006). a(254) can be used to character the optical properties of DOC aromaticity (Jaffe´ et al., 2004; Weishaar et al., 2003). The highest averaged CDOM absorption coefficients a(350), a(280), a(254) were also present in February 2014, corresponding to the highest DOC concentration. The S_R values of the two wavelength ranges (275-295 nm over 350-400 nm) were used to represent DOM molecular weight (Helms et al., 2008). The lowest mean of S_R was present in August 2013 suggesting the relatively weak microbial decomposition of plants and lots of terrestrially imported substances through rainwash resulted in the higher average molecular weight of DOC.

Table 3. Mean values of DOC concentration and CDOM absorption coefficients groups at different seasons. S_R: the slope ratio of $S_{275\text{-}295nm}$: $S_{350\text{-}400nm}$.

When the whole data set (N = 67) was pooled together, there were significantly positive linear relationships between a(254), a(280), a(350) and F_{max} for two humic-like components (C1 and C2), respectively, but mostly such correlations were not observed for the protein-like components (Fig. 4a and b, Table 3). These results were in accordance with previous investigations (Zhang et al., 2010, 2011). Components 1 and 2 were strongly linearly correlated with each other (R^2 = 0.633) (Fig. 4c), indicating that the concentrations of the two humic-like components were controlled by common sources (Baker and Spencer, 2004). There was a weak

404 relationship ($R^2 = 0.051$) between the protein-like components (C3 and C4) because of
405 a complex origin of CDOM such as rainfall in summer, ice in winter and organic
406 pollutants derived from domestic, agricultural and industrial sewerage, which
407 represent the complex origins of CDOM. However, there was almost no correlation
408 between the humic-like and protein-like components. The linkage of a fluorescence
409 signal to DOC was very complicated because of the seasonal impacts, i.e., increased
410 rainfall, algal blooms and ice-cover, which affect the DOC concentration. Due to both
411 steady and labile CDOM fluorescent components in DOC, the fluorescent signal
412 would changes with the ratio of fluorescent and non-fluorescent CDOM components
413 (Henderson et al., 2009). A weak relationship ($R^2 = 0.42$) (Fig. 4d) was found between
414 DOC and component 3 from the decay of plants through microbial activity or the
415 pollution from human and animal wastes.

416 Different from the findings by Yamashita et al. (2008) for ocean water, this study
417 did not find obvious correlation between salinity and EEM-PARAFAC extracted
418 components with the exception of C3 ($R^2 = 0.469$) (Table 4 and Fig. 4f). The most
419 important finding for the water samples collected at different seasons from the
420 Songnen Plain is a significant relationship ($R^2 = 0.931$) between salinity and DOC
421 (Fig. 4e). This is because DOC is evapo-condensed from spring to autumn and
422 freeze-accumulated in winter in the semi-arid region. A prolonged sunshine duration
423 can result in an evapo-condensed DOC concentration from April to August 2013. On
424 the other hand, the DOC is accumulated when the lakes freeze in winter leaving DOC
425 in the liquid phase.

426

427 **Table 4. Correlation coefficients (R) and significance levels (*p*) of the linear relationships**
428 **between CDOM absorption, DOC, salinity and fluorescent components.**

429

430 **Figure 4. Relationships between CDOM absorption coefficient a(350) with a) F_{max}(C1), b)**
431 **with F_{max}(C2), c) peak F_{max}(C1) versus F_{max}(C2), d) peak F_{max}(C3) versus DOC, e) Salinity**
432 **versus DOC, f) Salinity versus F_{max}(C3).**

433

434 # 4 Conclusions

435 A model II-ANOVA using season and lake as random effect factors shows that the
436 seasonal variability ($F > F_{crit}$, $p < 0.05$) is higher than between-lake variability. In this
437 study, the application of EEM-PARAFAC to characterize four fluorescent
438 components under seasonal variation in CDOM was presented with 67 water samples
439 collected from June 2013 to April 2014 in the semi-arid region of the Songnen Plain.
440 Two humic-like and the protein-like components were identified using PARAFAC
441 model. The average fluorescence intensity of the four components differed under
442 seasonal variation from June 2013 to April 2014. The highest C1 1.02 nm^{-1} was
443 presented in February 2014 due to the condensed CDOM caused by ice formation in
444 winter. Especially in summer when quantities of rainfall take place and in winter
445 when water is frozen, the fluorescence intensity is dominated by tyrosine-like
446 component in rain and ice-melt water. Component 1 and 2 exhibited strong linear
447 correlation ($R^2 = 0.633$). There were significantly positive linear relationships
448 between F_{max} and CDOM absorption coefficient a(254) ($R^2 = 0.72, 0.46$, $p < 0.01$),
449 a(280) ($R^2 = 0.77, 0.47$, $p < 0.01$), a(350) ($R^2 = 0.76, 0.78$, $p < 0.01$) for two

450 humic-like components (C1 and C2), respectively. A weak relationship (R^2 = 0.42)
451 was found between DOC and component 3 from the decay of plants through
452 microbial activity or the pollution from human and animal wastes. However, almost
453 no obvious correlation was found between salinity and EEM-PARAFAC extracted
454 components except C3 (R^2 = 0.469), though the correlation was not as strong as with
455 DOC concentration. Most importantly, a significant relationship (R^2 = 0.931) was
456 found between salinity and DOC. In order to understand the biogeochemical effects
457 on the aquatic ecosystem, further study should be required to identify CDOM source
458 and assess physical/chemical, bioavailable and photoreactive transformation in
459 various lakes with larger saline gradients in the semi-arid region, Northeast China.

460

461 **Acknowledgements**

462 The research was jointly supported by the "One Hundred Talents" program from
463 Chinese Academy of Sciences and the National Natural Science Foundation of China
464 (No. 41171293). The authors thank Zhi Ding, Ying Guan, Lei Liu and Ming Wang for
465 their persistent assistance with both field sampling and laboratory analysis.

466

467 **References**

468 APHA/AWWA/WE F.: Standard Methods for the Examination of Water and
469 Wastewater, Washington, DC: American Public Health Associstion, 1998.
470 Aiken, G. R., McKnight, D. M., Thorn, K. A., and Thurman, E. M.: Isolation of

hydrophobic organic-acids from water using nonionic macro porous resins, Org. Geochem., 18, 567-573, 1992.

Andersen, C. M., and Bro, R.: Practical aspects of PARAFAC modeling of fluorescence excitation-emission data, J. Chemom., 17, 200-215, 2003.

Andersso, C. A., and Bro. R.: The N-way Toolbox for MATLAB, Chemom. Intell. Lab. Syst., 52, 1–4, 2000.

Babin, M., Stramski, D., Ferrari, G. M., Claustre, H., Bricaud, A., Obolensky, G., and Hoepffner, N.: Variations in the light absorption coefficients of phytoplankton, nonalgal particles, and dissolved organic matter in coastal waters around Europe, J. Geophys. Res., 108, 3211-3230, 2003.

Baker, A., Ward, D., Lieten, Shakti H., Periera, R., Simpson, Ellie C., and Slater, M.: Measurement of protein-like fluorescence in river and waste water using a handheld spectrophotometer, Water Res., 38, 2934-2938, 2004.

Baker, A., and Spencer, R. G. M.: Characterization of dissolved organic matter from source to sea using fluorescence and absorbance spectroscopy, Sci. Total Environ., 333, 217-232, 2004.

Barker, J. D., Dubnick, A., Lyons, W. B., and Chin, Y. P.: Changes in Dissolved Organic Matter (DOM) Fluorescence in Proglacial Antarctic Streams, Arct. Antarct. Alp. Res., 45, 305-317, 2013.

Barker, J. D., Sharp, M. J., Fitzsimons, S. J., and Turner, R. J.: Abundance and dynamics of dissolved organic carbon in glacier systems, Arct. Antarct. Alp. Res.,

492 38, 163–172, 2006.

493 Barker, J. D., Sharp, M. J., and Turner, R. J.: Using synchronous fluorescence
494 spectroscopy and principal components analysis to monitor dissolved organic
495 matter dynamics in a glacier system, Hydrol. Processes, 23, 1487–1500, 2009.

496 Barker, J. D., Klassen, J. L., Sharp, M. J., Fitzsimons, S. J., and Turner, R. J.:
497 Detecting biogeochemical activity in basal ice using fluorescence spectroscopy,
498 Ann. Glaciol., 51, 47–55, 2010.

499 Borisover, M., Laor, Y., Parparov, A., Bukhanovsky, N., and Lado, M.: Spatial and
500 seasonal patterns of fluorescent organic matter in Lake Kinneret (Sea of Galilee)
501 and its catchment basin, Water Res., 43, 3104-3116, 2009.

502 Bricaud, A., Babin, M., Morel, A., and Claustre, H.: Variability in the
503 chlorophyll-specific absorption coefficients of natural phytoplankton: Analysis
504 and parameterization, J. Geophys. Res., 100, 13321–13332, 1995.

505 Bro, R.: PARAFAC tutorial and applications, Chemom. Intell. Lab. Syst., 38, 149-171,
506 1997.

507 Bro, R.: Exploratory study of sugar production using fluorescence spectroscopy and
508 multi-way analysis, Chemom. Intell. Lab. Syst., 46,133-147, 1999.

509 Cheng, Y. Y., Guo, W. D., Long, A. M., and Chen, S. Y.: Study on optical
510 characteristic of chromophoric dissolved organic matter in rainwater by
511 fluorescence excitation-emission matrix and absorbance spectroscope (Article in
512 Chinese), Spectrosc. Spect. Anal., 30, 2413-2416, 2010.

513 Coble, P. G.: Characterization of marine and terrestrial DOM in seawater using
514 excitation-emission matrix spectroscopy, Mar. Chem., 51, 325–346, 1996.

515 Coble, P. G.: Marine optical biogeochemistry: the chemistry of ocean color, Chem.
516 Rev., 107, 402-418, 2007.

517 Coble, P. G., Del Castillo, C. E., and Avril, B.: Distribution and optical of CDOM in
518 the Arabian Sea during the 1995 Southwest Monsoon, Deep-Sea Res. part II, 45,
519 2195–2223, 1998.

520 Cory, R. M., and McKnight, D. M.: Fluorescence spectroscopy reveals ubiquitous
521 presence of oxidized and reduced quinines in dissolved organic matter, Environ.
522 Sci. Technol., 39, 8142-8149, 2005.

523 DelCastillo, C. E., Coble, P. G., Morell, J. M., Lopez, J. M., and Corredor, J. E.:
524 Analysis of the optical propertiesof the Orinoco River plume by absorption and
525 fluorescence spectroscopy, Mar. Chem., 66, 35–51, 1999.

526 Fellman, J. B., Hood, E., and Spencer, R. G. M.: Fluorescence spectroscopy opens
527 new windows into dissolved organic matter dynamics in freshwater ecosystems:
528 A review, Limnol. Oceanogr., 55, 2452-2462, 2010.

529 Guo, W. D., Xu, J., Wang, J. P., Wen, Y. G., Zhou, J. F., and Yan, Y. C.:
530 Characterization of dissolved organic matter in urban sewage using excitation
531 emission matrix fluorescence spectroscopy and parallel factor analysis, J.
532 Environ. Sci., 22, 1728-1734, 2010.

533 Henderson, R. K., Baker, A., Murphy, K. R., Hambly, A., Stuetz, R. M., and Khan, S.

534 J.: Fluoresence as a potential monitoring tool for recycled water system: A
535 review, Water Res., 43, 863-881, 2009.
536 Helms, J. R., Stubbins, A., Ritchie, J. D., Minor, E. C., Kieber, D. J., and Mopper, K.:
537 Absorption spectral slopes and slope ratios as indicators of molecular weight,
538 source, and photo bleaching of chromophoric dissolved organic matter, Limnol.
539 Oceanogr., 53, 955–969, 2008.
540 Hua, B., Dolan, F., Mcghee, C., Clevenger, ThomasE., and Deng, B. L.: Water-source
541 characterization and classification with fluorescence EEM spectroscopy:
542 PARAFAC analysis, Int. J. Environ. Anal. Chem., 87, 135-147, 2007.
543 Hudson, N., Baker, A., and Reynolds, D.: Fluorescence analysis of dissolved organic
544 matter in natural, waste and polluted waters – a review, River Res. Appl., 23,
545 631–649, 2007.
546 Jaffe´, R., Boyer, J. N., Lu, X., Maie, N., Yang, C., Scully, N. M., and Mock, S.:
547 Source characterization of dissolved organic matter in subtropical
548 mangrove-dominated estuary by fluorescence analysis, Mar. Chem., 84, 195–210,
549 2004.
550 Larsson, T., Wedborg, M., and Turner, D.: Correction of inner-filter effect in
551 fluorescence excitation-emission matrix spectrometry using Raman scatter, Anal.
552 Chim. Acta., 583, 357-363, 2007.
553 Lawaetz, A. J., and Stedmon, C. A.: Fluorescence Intensity Calibration Using the
554 Raman Scatter Peak of Water, Appl. Spectrosc., 63, 936-940, 2009.

555 Mayer, L. M., Schick, L. L., and Loder, T. C.: Dissolved protein fluorescence in two
556 Maine estuaries, Mar. Chem., 64, 171–179, 1999.

557 McDowell, W. H., Zsolnay, A., Aikenhead-Peterson, J. A., Gregorich, E. G., Jones, D.
558 L., Jo¨dermann, D., Kalbitz, K., Marschner, B., and Schwesig, D.: A
559 comparison of methods to determine the biodegradable dissolved organic
560 carbon from different terrestrial sources, Soil Biol. Biochem., 38, 1933–1942,
561 2006.

562 Mcknight, D. M., Boyer, E. W., Westerhoff, P. K., Doran, P. T., Kulbe, T., and
563 Andersen, D. T.: Spectrofluorometriccharacterization of dissolved organic
564 matter for indication of precursor organic material and aromaticity, Limnol.
565 Oceanogr., 46, 38–48, 2001.

566 Song, C. C., Wang, L. L., Guo, Y. D., Song, Y. Y., Yang, G. S., and Li, Y. C.: Impacts
567 of natural wetland degradation on dissolved carbon dynamics in the Sanjiang
568 Plain, Northeastern China, J. Hydrol., 398, 26-32, 2011.

569 Song, K. S., Zang, S. Y., Zhao, Y., Du, J., Lin, L., Zhang, N. N., Wang, X. D., Shao, T.
570 T., Guan, Y., and Liu, L.: Spatiotemporal characterization of dissolved carbon
571 for inland waters in semi-humid/semiarid region, China, Hydrol. Earth Syst.
572 Sci., 17, 4269-4281, 2013.

573 Spencer, R. G. M., Hernes, P. J., Ruf, R., Baker, A., Dyda, R. Y., Stubbins, A., and
574 Six, J.: Temporal controls on dissolved organic matter and lignin
575 biogeochemistry in apristine tropical river, J. Geophys. Res. Biogeosci., 115,

G03013, 2010.

Stedmon, C. A., and Bro, R.: Characterizing dissolved organic matter fluorescence with parallel factor analysis: a tutorial, Limnol. Oceanogr. Methods, 6, 572-579, 2008.

Stedmon, C. A., and Markager, S.: Tracing the production and degradation of autochthonous fractions of dissolved organic matter by fluorescence analysis, Limnol. Oceanogr., 50, 1415-1426, 2005.

Stedmon, C. A., Markager, S., and Bro, R.: Tracing dissolved organic matter in aquatic environments using a new approach to fluorescence spectroscopy, Mar. Chem., 82, 239-254, 2003.

Stedmon, C. A., Thomas, D. N., Granskog, M., Kaartokallio, H., Papadimitriou, S., and Kuosa, H.: Characteristics of dissolved organic matter in Baltic coastal sea ice: allochthonous or autochthonous origins? Environ. Sci. Technol., 41, 7273–7279, 2007.

Thomas K. B.: Under Landfast ice, Arctic, 36, 328-340, 1983.

Uusikiv, J., Vahatal, A.V., Granskog, M.A., Sommaruga, R., 2010. Contribution of mycosporine-like amino acids and colored dissolved and particulate matter to sea ice optical properties and ultraviolet attenuation, Limnol. Oceanogr., 55(2), 703–713.

UV talk letter vol. 10, 2013. https://shimadzu.com.au/uv-talk-letter-volume-10

Weishaar, J. L., Aiken, G. R., Bergamaschi, B. A., Farm, M. S., Fujii, R., and Mopper,

597 K.: Evaluation of specific ultraviolet absorbance as an indicator of the chemical
598 composition and reactivity of dissolved organic carbon, Environ. Sci. Technol.,
599 37, 4702– 4708, 2003.
600 Wharton, R. A., Jr., McKay, C. P., Clow, G. D., and Andersen, D. T.: Perennial ice
601 covers and their influence on Antarctic lake ecosystems, Antarct. Res. Ser., 59,
602 53–70, 1993.
603 Yamashita, Y.: Assessing the dynamics of dissolved organic matter (DOM) in coastal
604 environments by excitation emission matrix fluorescence and parallel factor
605 analysis (EEM-PARAFAC), Limnol. Oceanogr., 53, 1900-1908, 2008.
606 Yamashita, Y., Cory, R. M., Nishioka, J., Kuma, K., Tanoue, E., and Jaffe´, R.,:
607 Fluorescence characteristics of dissolved organic matter in the deep waters of the
608 Okhotsk Sea and the northwestern North Pacific Ocean, Deep Sea Res. Part II,
609 57, 1478–1485, 2010.
610 Zhang, Y. L., Liu, X. H., Osburn, C. L., Wang, M. Z., Qin, B. Q., and Zhou, Y. Q.:
611 Photo bleaching response of different Source of Chromophoric Dissolved
612 Organic Matter Exposed to Natural Solar Radiation Using Absorption and
613 Excitation-Emission Matrix Spectra, Plos one, 8, e77515, 2013.
614 Zhang, Y. L., Yin, Y., Feng, L. Q., Zhu, G. W., Shi, Z. Q., Liu, X. H., and Zhang, Y. Z.:
615 Characterizing chromophoric dissolved organic matter in Lake Tianmuhu and its
616 catchment basin using excitation-emission matrix fluorescence and parallel
617 factor analysis, Water Res., 45, 5110-5122, 2011.

618 Zhang, Y. L., Zhang, E. L., Yin, Y., VanDijk, M. A., Feng, L. Q., Shi, Z. Q., Liu, M. L.,
619 and Qin, B. Q.: Characteristics and sources of chromophoric dissolved organic
620 matter in lakes of the Yungui Plateau, China, differing in trophic state and
621 altitude, Limnol. Oceanogr., 55, 2645-2659, 2010.
622 Zhang, Y. L., VanDijk, M. A., Liu, M. L., Zhu, G. W., and Qin, B. Q.: The
623 contribution of phytoplankton degradation to chromophoric dissolved organic
624 matter (CDOM) in eutrophic shallow lakes: Field and experimental evidence.
625 Water Res., 43, 4685–4697, 2009.
626
627
628
629
630
631
632
633
634
635
636
637
638
639
640
641
642
643
644

Table 1. Mean value of water quality parameters from June 2013 to April 2014. Turb denotes water turbidity; N denotes sampling numbers.

Sampling season	pH	Salinity (PSU)	Turb (NTU)	N
Jun.2013	8.54	0.40	166.20±108.73	15
Aug.2013	8.63	0.37	63.13±31.21	13
Feb.2014	8.35	0.70	21.33±15.87	17
Apr.2014	8.67	0.43	22.24±16.42	22
All	8.55	0.48	62.18±79.07	67

Table 2. Positions of the fluorescence maximum peaks of the four components identified by PARAFAC modeling in the present study compared with those previously identified. Secondary excitation maxima is given in brackets.

Component No	Ex_{max}(nm)	Em_{max}(nm)	Description and source	Components (Coble) and (Zhang)	Components (Stedmon and Markager)
C1	230 (300)	425	Marine humic-like (phytoplankton degradation)	M	6
C2	255 (350)	460	Terrstrial humic-like	A and C	1 and 4
C3	225 (290)	360	Autochthonous tryptophan-like	T	
C4	220 (275)	320	Autochthonous tyrosine-like	B	8

Fluoresence peaks were named as Components (Coble) and (Zhang) by Coble et al. (1996, 1998) and Zhang et al. (2010, 2011), while as Componets (Stedmon and Markager) by Stedmon and Markager (2005).

693

694 Table 3. Mean values of DOC concentration and CDOM absorption coefficients
695 groups at different seasons. S_R: the slope ratio of $S_{275\text{-}295nm}$: $S_{350\text{-}400nm}$.
696

Sampling season	a(254) m^{-1}	a(280) m^{-1}	a(350) m^{-1}	S_R	DOC mg L^{-1}	N
Jun.2013	38.39±9.23	25.98±6.38	5.73±1.68	1.29±0.16	31.84±14.67	15
Aug.2013	29.71±4.73	19.36±2.91	5.82±0.81	0.96±0.22	32.83±14.78	13
Feb.2014	52.88±18.13	34.62±11.54	6.36±2.17	1.18±0.11	55.04±20.00	17
Apr.2014	34.43±11.38	22.45±7.36	4.17±1.49	1.32±0.13	30.86±10.91	22
All	39.08±14.73	25.73±9.58	5.40±1.84	1.21±0.20	37.60±18.05	67

697
698
699
700
701
702
703
704
705
706
707
708
709
710
711
712
713
714

715

716 Table 4. Correlation coefficients (R) and significance levels (*p*) of the linear
717 relationships between CDOM absorption, DOC, salinity and fluorescent components.

718

	a(254)	a(280)	a(350)	DOC	Salinity	C1	C2	C3	C4
DOC	0.711**	0.646**	0.294*	1.000**					
Salinity	0.650**	0.579**	0.159	0.965**	1.000**				
C1	0.850**	0.875**	0.873**	0.496**	0.383**	1.000**			
C2	0.677**	0.686**	0.885**	0.414**	0.270*	0.796**	1.000**		
C3	0.452**	0.417**	0.134	0.648**	0.685**	0.267*	0.103	1.000**	
C4	-0.040	-0.016	0.078	-0.101	0.135	0.084	0.069	0.225	1.000**

719 **p< 0.01 level ; *p<0.05 level.

720

721

722

723

724

725

726

727

728

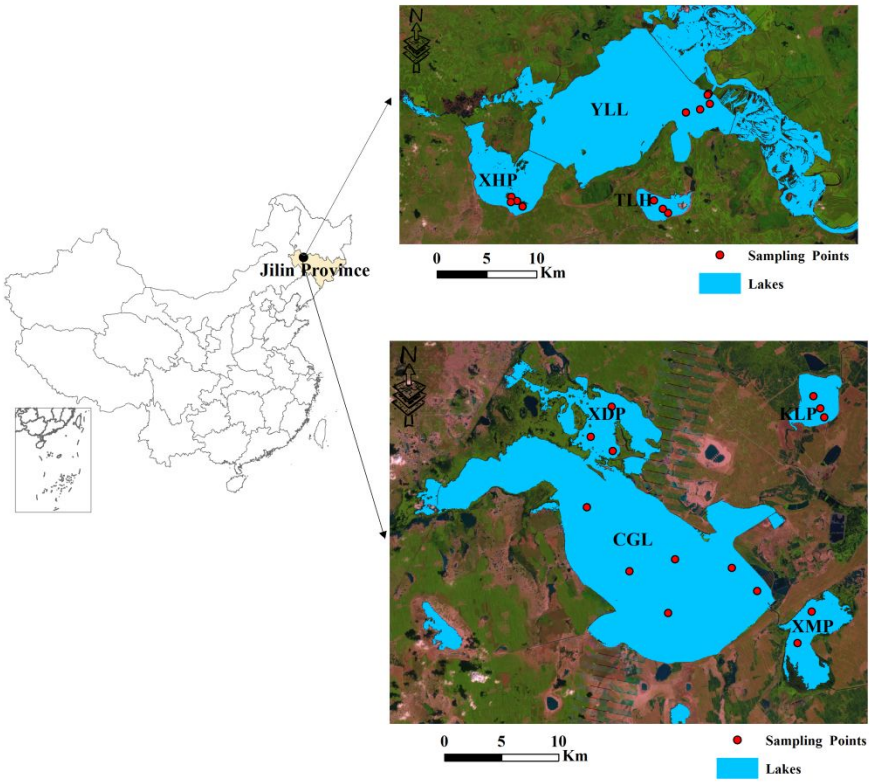

729
730
731

732 Figure 1. Locations of the water sampling sites for 7 lakes in the western part of Jilin

733 province, Northeast China.

734

735

736

737

738

739

740

741

742

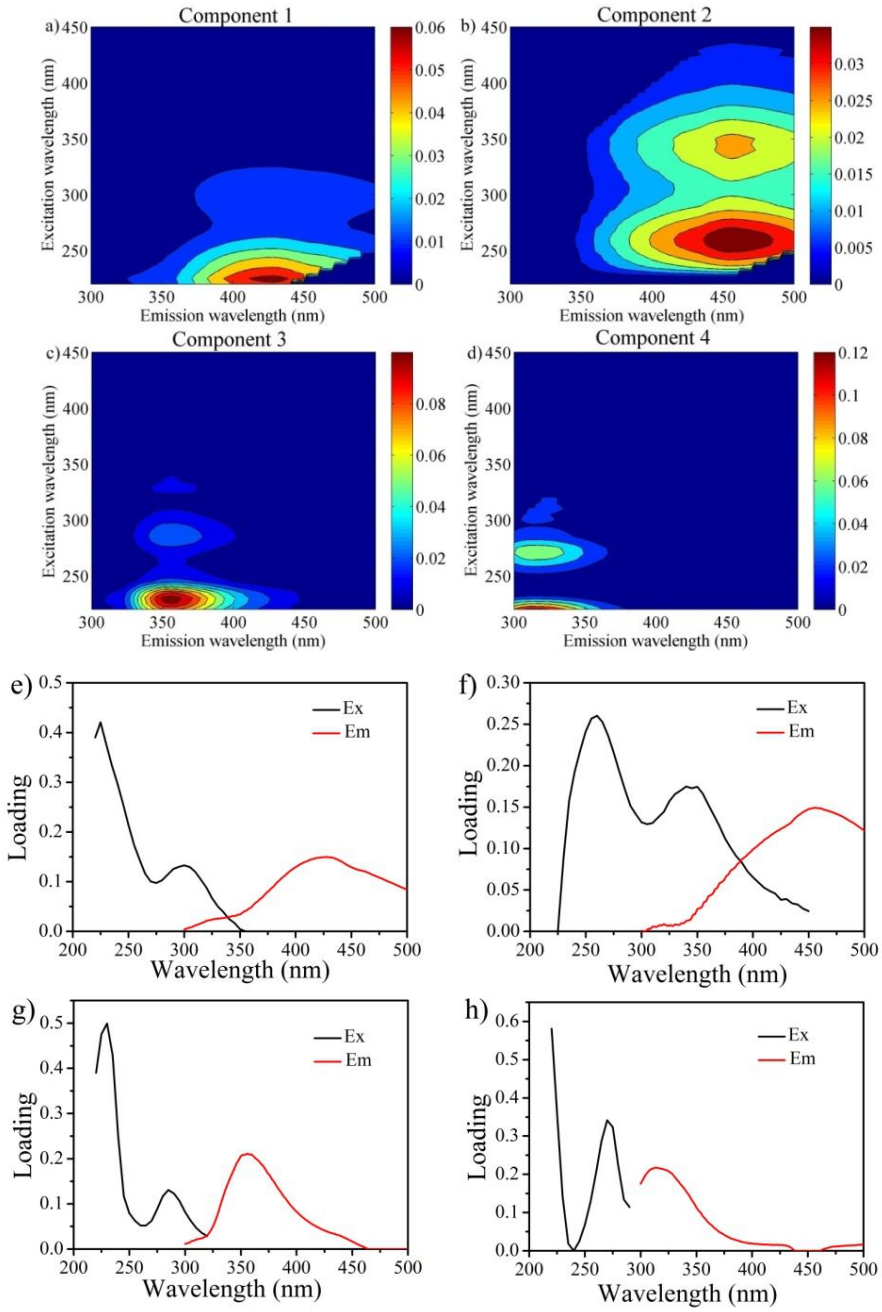

Figure 2. The PARAFAC model output shows the contour plots of the four PARAFAC fluorescent components (a-d) and excitation (black) and emission (red) loadings (e-h) of each component. Fluorescence is in Raman units: nm^{-1}.

765

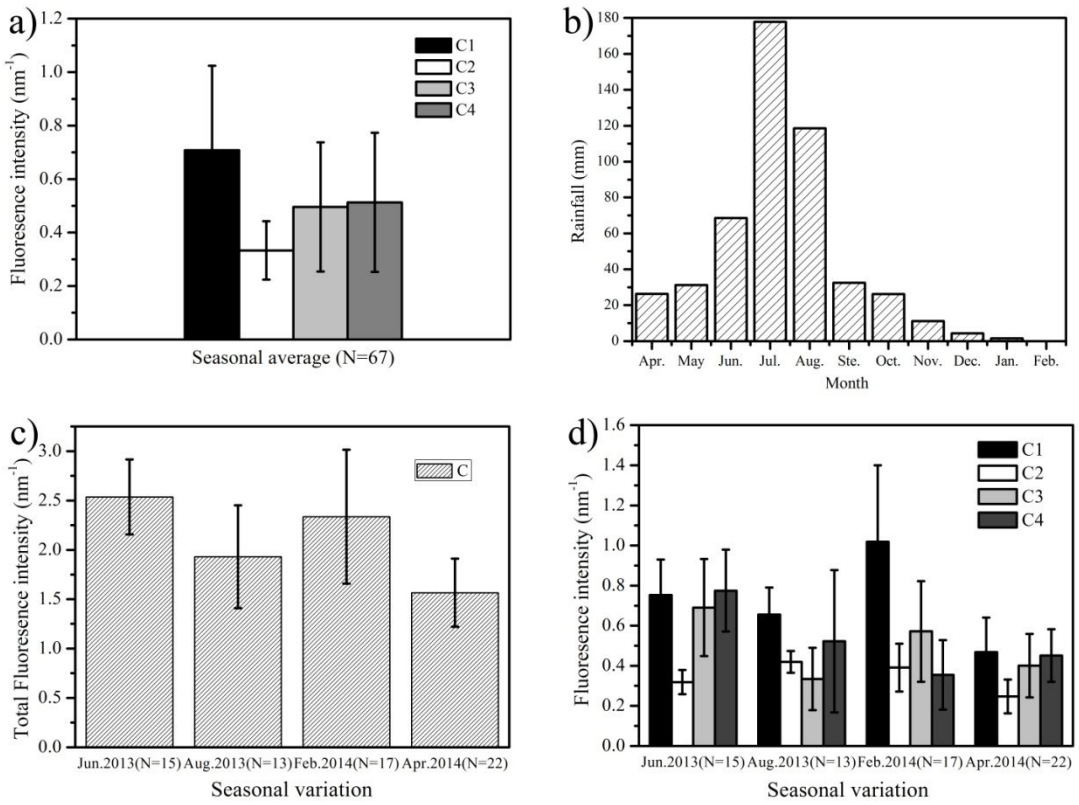

766

767 Figure 3. a) Seasonal average of F_{max} for EEM-PARAFAC components (C1, C2, C3
768 and C4) for lakes in the western part of Jilin province; b) Monthly variation of rainfall
769 for the lakes in western part of Jilin province from April 2013 to February 2014; c)
770 Seasonal variation of the total fluorescence intensity at different seasons; d) Seasonal
771 variation of the four EEM-PARAFAC components at different seasons; The error bar
772 represents standard deviations.

773

774

775

776

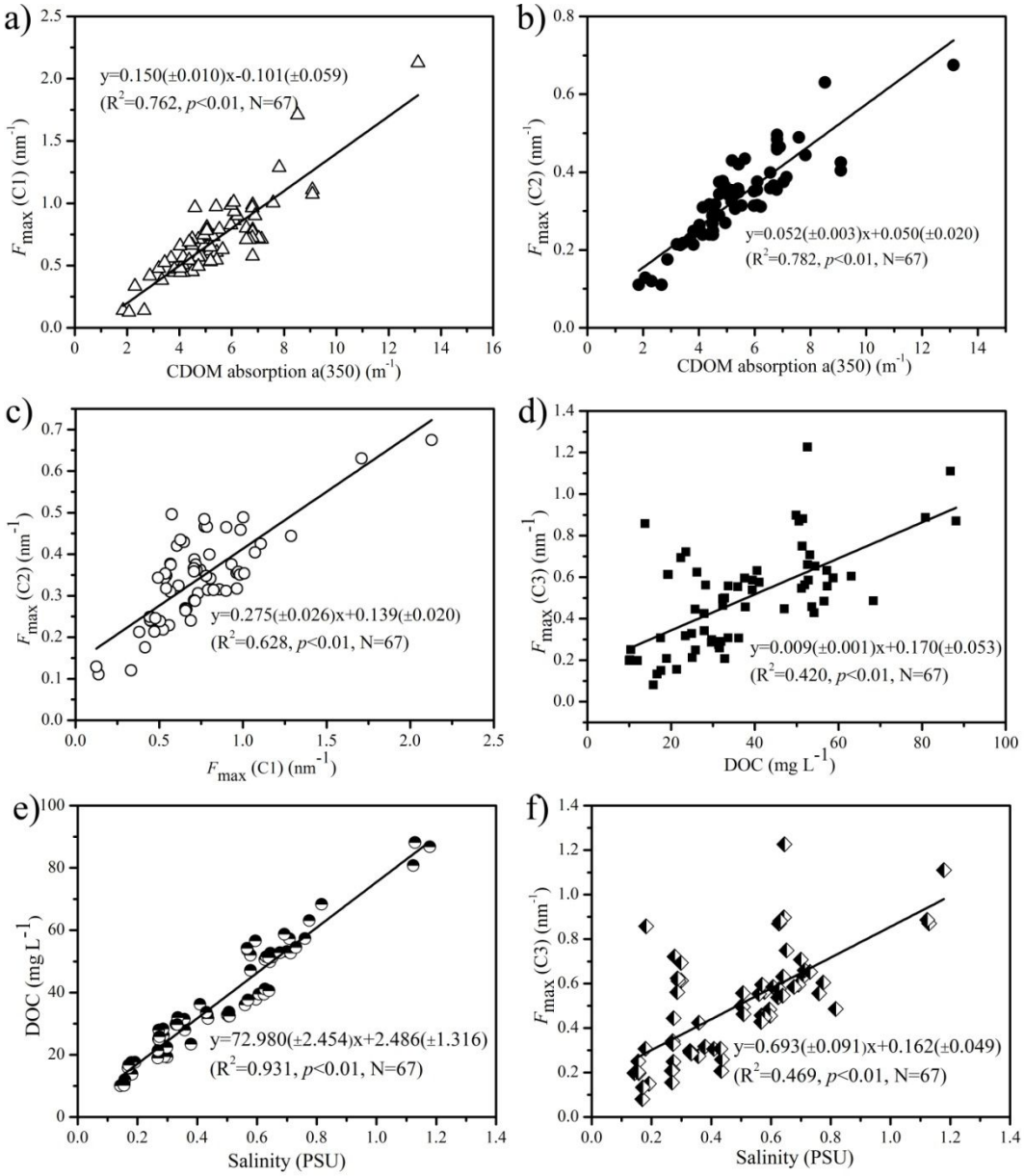

Figure 4. Relationships between CDOM absorption coefficient a(350) with a) F_{max}(C1), b) with F_{max}(C2), c) F_{max}(C1) versus F_{max}(C2), d) F_{max}(C3) versus DOC, e) Salinity versus DOC, f) Salinity versus F_{max}(C3).

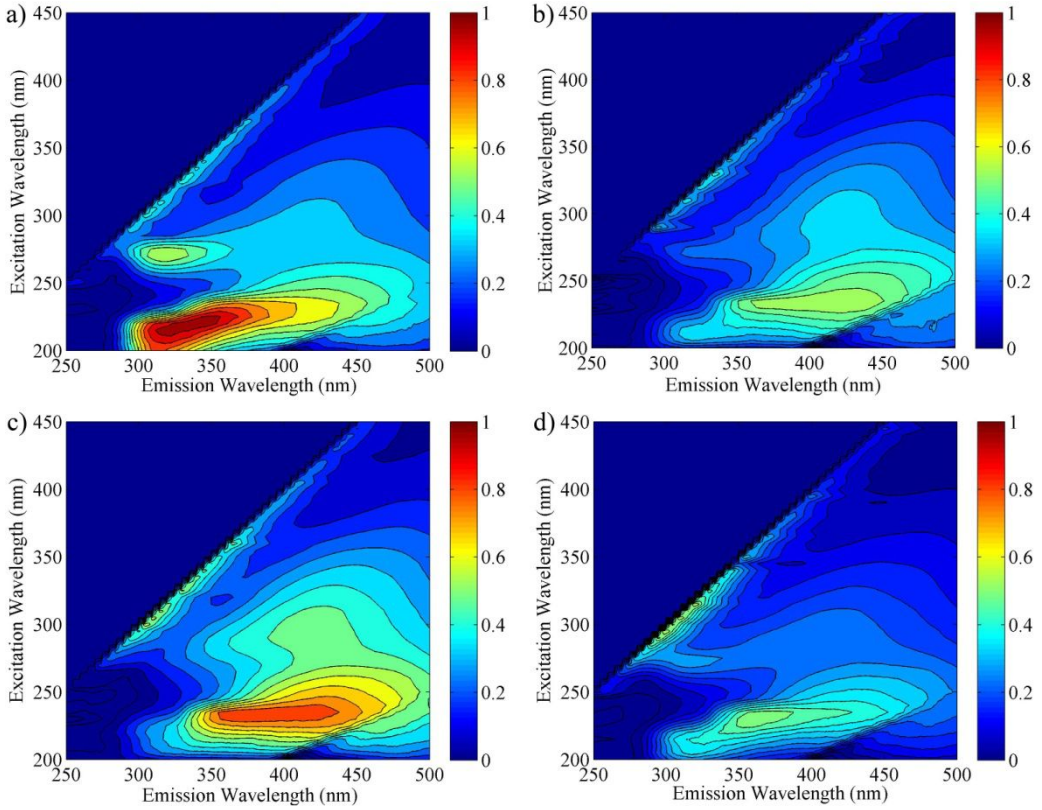

Figure S1. Examples of EEMs for one water sample from Xindianpao Lake in the western part of Jilin province at different seasons a) June 2013; b) August 2013; c) February 2014; d) April 2014 (Fluorescence is in Raman unit: nm^{-1}).

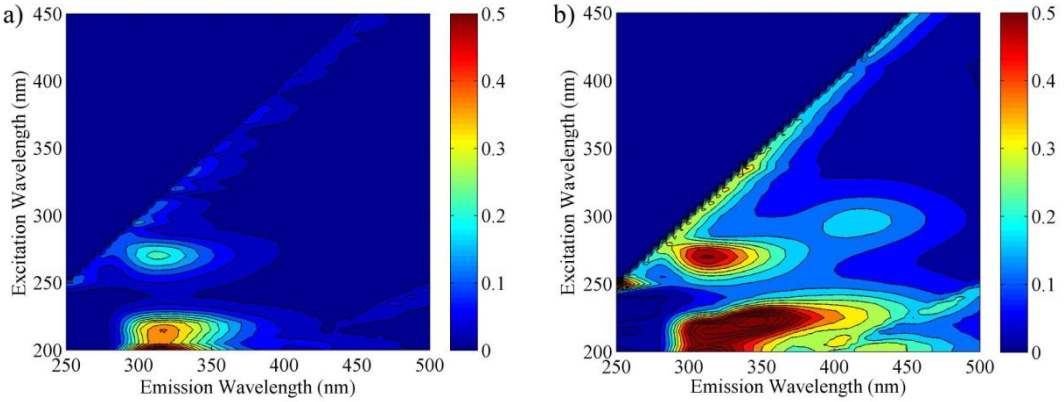

Figure S2. Representative examples of EEMs for a) lake ice-melt water sample, and b) rainwater CDOM in the western part of Jilin province (Raman: nm^{-1}).